Quantum Dynamical Simulation of Intramolecular Singlet Fission in Covalently Coupled Pentacene Dimers

S. Rajagopala Reddy,[1] Pedro B. Coto,[2] and Michael Thoss[1]

[1] *Institute of Physics, Albert-Ludwigs University Freiburg, Hermann-Herder-Str. 3, 79104 Freiburg, Germany*[a]

[2] *Department of Physical and Analytical Chemistry, University of Oviedo, Oviedo, Spain*[b]

We analyze the dynamics of intramolecular singlet fission in a series of pentacene-based dimers consisting of two pentacene-like chromophores covalently bonded to a phenylene linker in *ortho*, *meta* and *para* positions. The study uses a quantum dynamical approach that employs a model vibronic Hamiltonian whose parameters are obtained using multireference perturbation theory methods. The results highlight the different role of the direct and mediated mechanism in these systems, showing that the population rate of the multiexcitonic state, corresponding to the first step of the intramolecular singlet fission process, occurs mainly through a superexchange-like mechanism involving doubly excited or charge transfer states that participate in the process in a virtual way. In addition, the systems investigated provide insight into roles that built-in geometrical constraints and the electronic structure of the spacer play in the intramolecular singlet fission process.

[a] Electronic mail: michael.thoss@physik.uni-freiburg.de

[b] Electronic mail: branapedro@uniovi.es

I. INTRODUCTION

The last years have witnessed a renewed interest in the investigation of singlet fission (SF).[1–3] This photophysical process, first invoked in the 1960s to explain the appearance of delayed fluorescence in some organic molecular crystals,[4,5] has re-emerged as an active research topic in the context of energy conversion.[6,7] The main reason for this is that SF, being a charge carrier multiplication process,[8] bears the potential to improve the efficiency of solar cells[9,10] by circumventing the limitation imposed by the Shockley-Queisser limit.[6,7,11] Systems exhibiting SF can bypass this limitation by generating two charge carriers out of a single photon absorption. Considering, for example, a dimer of chromophores initially in the ground state ($|^1(S_0S_0)\rangle$), light absorption triggers excitation of one of the chromophors to a low-lying singlet excited state ($|^1(S_1S_0)\rangle$). This state ultimately transforms into a pair of separate, non-interacting triplet excitons ($|T_1\rangle |T_1\rangle$), where each of them can eventually generate a charge carrier. In the SF process, the emerging $|T_1\rangle |T_1\rangle$ state is initially coupled forming a singlet state $|^1(T_1T_1)\rangle$, the so-called multiexciton (ME) state) so this step of the process is spin-allowed.[1,12–15] Subsequent evolution controlled by the magnetic dipole-dipole interaction leads to the formation of separate, triplet excitons in a process where several states of different spin multiplicity interact in a complex interplay.[1,16–25] The complexity of the process has motivated an important theoretical research effort to decipher SF, which implies identifying the electronic states participating in the process, their roles[23–41] and coupling mechanisms[1,42–51] and characterizing the dynamics, including the role of mode specific aspects of the nuclear motion, conical intersections, interference and decoherence effects.[14,15,28,40,41,43,47,52–74]

As a result of this collective research effort, key electronic and structural parameters controlling SF at the molecular level[1–3,13,50,55,75–84] as well as detailed information on the mechanism of the process[1–3] have been identified. Specifically, it has been shown that to achieve spontaneous SF and minimize quenching processes the electronic states of the chromophores involved in the process have to fulfill several energy relationships.[1] Furthermore, two reaction channels have been invoked to rationalize the process of SF, the direct and the mediated mechanism.[1] In the direct mechanism, the transformation of the initially populated singlet excited state into the ME state that eventually dissociates into two uncoupled $|T_1\rangle$ states does not involve the participation of other states. In contrast, in the mediated

mechanism, this transformation involves the participation of high-lying charge transfer (CT) states whose mixing with the optically excited and the ME states mediates the population of the latter. Although new experimental findings have led to the proposal of alternative mechanisms, where the nature of the electronic states taking part in the process[28,85] or the type and number of intermediates involved[21–25,86] depart from those of the traditional reaction channels, these retain a central role in most discussions dealing with the SF mechanism.

In this context, the mechanism of intramolecular SF (iSF) in solution has been recently investigated in a series of 6,13-bis(triisopropylsilylethynyl)pentacene-derived (TIPSP) dimers covalently bonded to a phenylene spacer in *ortho*, *meta*, and *para* positions using a combination of time-resolved spectroscopic techniques and multireference perturbation theory calculations.[34] The motivation underlying this research was twofold. On the one hand, iSF can potentially be used for the development of solution-processable SF-based photovoltaic devices[87] and therefore its characterization provides instrumental information for their design. On the other hand, the use of this type of molecules facilitates the identification of the intrinsic molecular aspects underlying the iSF mechanism. This is achieved through (i) the built-in geometrical constraints that enable control of the through-space and through-bond couplings, and their contributions to the effective iSF coupling[34,88] and (ii) the existence of specific molecular vibrations that are known to play an all important role in the SF process.[31,37,42,89] As a result, it could be shown that in benzonitrile, the *ortho* regioisomer exhibits the fastest iSF process followed by *para* and *meta*. Furthermore, it was suggested that mixing of the absorbing state with higher-lying CT states could be one of the underlying reasons for this behavior.

To verify this hypothesis, we have recently investigated the dynamics of iSF using multireference perturbation theory and quantum dynamical methods with a simplified model of the *o*-TIPSP dimer.[70] The results obtained were qualitatively in line with those experimentally found, showing sizable population of the ME state in a sub-300 fs timescale. It was also shown that the population of the ME state proceeds *via* a mediated-like mechanism, with high-lying CT and DE virtual states acting in a superexchange-like way. Furthermore, the role of molecular vibrations in the iSF process was exposed, showing that a few high-frequency ring-breathing- and stretching-like vibrational modes were behind the modulation of the effective iSF coupling.

In this work, we build on these results and carry out a comparative study of the iSF

dynamics in simplified models of o-, m- and p-TIPSP dimers with the aim of assessing the impact that built-in constraints, specifically position isomerism and type of conjugation through the phenylene linker, have in the initial events of the iSF process.

II. METHODS

For the simulation of the dynamics of iSF in o-, m- and p-TIPSP we have used an approach that combines *ab-initio* and quantum dynamical methods. Specifically, we have used a vibronic model Hamiltonian[90] represented in a basis of diabatic states to describe the iSF process and employed the multilayer multiconfiguration time-dependent Hartree (ML-MCTDH) method[91–98] to solve the time-dependent Schrödinger equation. Within this approach, the Hamiltonian reads ($\hbar = 1$)

$$H = \sum_I H_I \, |I\rangle\langle I| + \sum_{I>J} (V_{I,J} \, |I\rangle\langle J| + \text{h.c.}), \tag{1}$$

where h.c. stands for Hermitian conjugate, I and J label diabatic electronic states and where the diagonal and off-diagonal vibronic terms are

$$H_I = E_I^0 + \sum_l \frac{\omega_l}{2}(Q_l^2 + P_l^2) + \sum_l (\kappa_{I,I}^l Q_l + \frac{1}{2}\gamma_{I,I}^l Q_l^2) \tag{2}$$

and

$$V_{I,J} = V_{I,J}^0 + \sum_l (\kappa_{I,J}^l Q_l + \frac{1}{2}\gamma_{I,J}^l Q_l^2). \tag{3}$$

Here, E_I^0 and $V_{I,J}^0$ stand for the energies of the diabatic electronic states considered in the model and their electronic couplings, respectively, obtained calculating the diabatic electronic Hamiltonian (H_{el}) at the ground state reference geometry of the system of interest. Q_l and P_l are the (dimensionless) coordinates and momenta of the vibrational degrees of freedom included in the simulations, ω_l are the corresponding harmonic frequencies and $\sum_l \frac{\omega_l}{2}(Q_l^2 + P_l^2)$ is the energy of the vibrational energy in the harmonic approximation. Finally, the rest of terms correspond to the first and second order vibronic couplings, where $\kappa_{I,J}^l$ and $\gamma_{I,J}^l$ denote the linear and quadratic coupling constants for mode l, respectively. In the calculations discussed below, 28, 29 and 26 vibrational normal modes were included for o-, m- and p-TIPSP, respectively, selected on the basis of the magnitude of their respective dimensionless coupling strengths ($\frac{\kappa^2}{2\omega^2}$, see Supporting Information).[90]

Using the model Hamiltonian defined above, we can obtain the dynamics of the population of the different states involved in the iSF process, which is given by

$$P_L(t) = \text{Tr} \{P_L \rho(t)\}, \tag{4}$$

where $P_L = |L\rangle\langle L|$ denotes the projector onto the diabatic electronic state $|L\rangle$ and

$$\rho(t) = e^{-iHt} \rho(0) e^{iHt} \tag{5}$$

the density matrix at time t. In our simulations, we have assumed that the initial state is prepared *via* an instantaneous optical excitation and that temperature effects on this state are negligible. Under these assumptions, the density matrix at $t = 0$ is given by

$$\rho(0) = |I\rangle |0_0\rangle\langle 0_0| \langle I|, \tag{6}$$

where $|I\rangle$ is the excited electronic state initially populated after optical excitation and $|0_0\rangle$ is the vibrational ground state of the electronic ground state of the system. In our model, we assume that only one of the diabatic LE states gets populated upon optical excitation. However, a short laser pulse would produce a delocalized initial state corresponding to a superposition of the two LE states for the systems investigated (see the corresponding energies and couplings in subsection III A). However, as the dynamics obtained for starting in either of the two LE states are very similar (see Supporting Information), we will in the following only present results obtained with an initial excitation of the lowest-lying diabatic state.

In addition to the electronics dynamics, we have also calculated the Fourier transform of the autocorrelation function of the initially excited state,

$$C(t) = \langle 0_0| \langle I| e^{-iHt} |I\rangle |0_0\rangle, \tag{7}$$

which provides the photoabsorption cross-section and can be compared with the experimental absorption spectra of the systems investigated.

The parameters needed to build the vibronic model Hamiltonian, namely the diabatic electronic states, their energies and electronic couplings, the harmonic modes and frequencies, and the vibronic coupling constants, were obtained using *ab-initio* methods as reported in ref. 70. In detail, the ground state equilibrium structures[34] of simplified models of o-, m- and p-TIPSP, with the triisopropylsilyl moieties replaced with methyl groups

(o-TIPSPm, m-TIPSPm and p-TIPSPm, see Fig. 1), were obtained using density functional theory (DFT), employing the B3LYP exchange-correlation functional[99–102] and the def2-TZVP basis set.[103] Dispersion interactions were taken into account using Grimme's approach.[104] Harmonic frequencies and normal modes for all the equilibrium structures were calculated at the same level of theory.
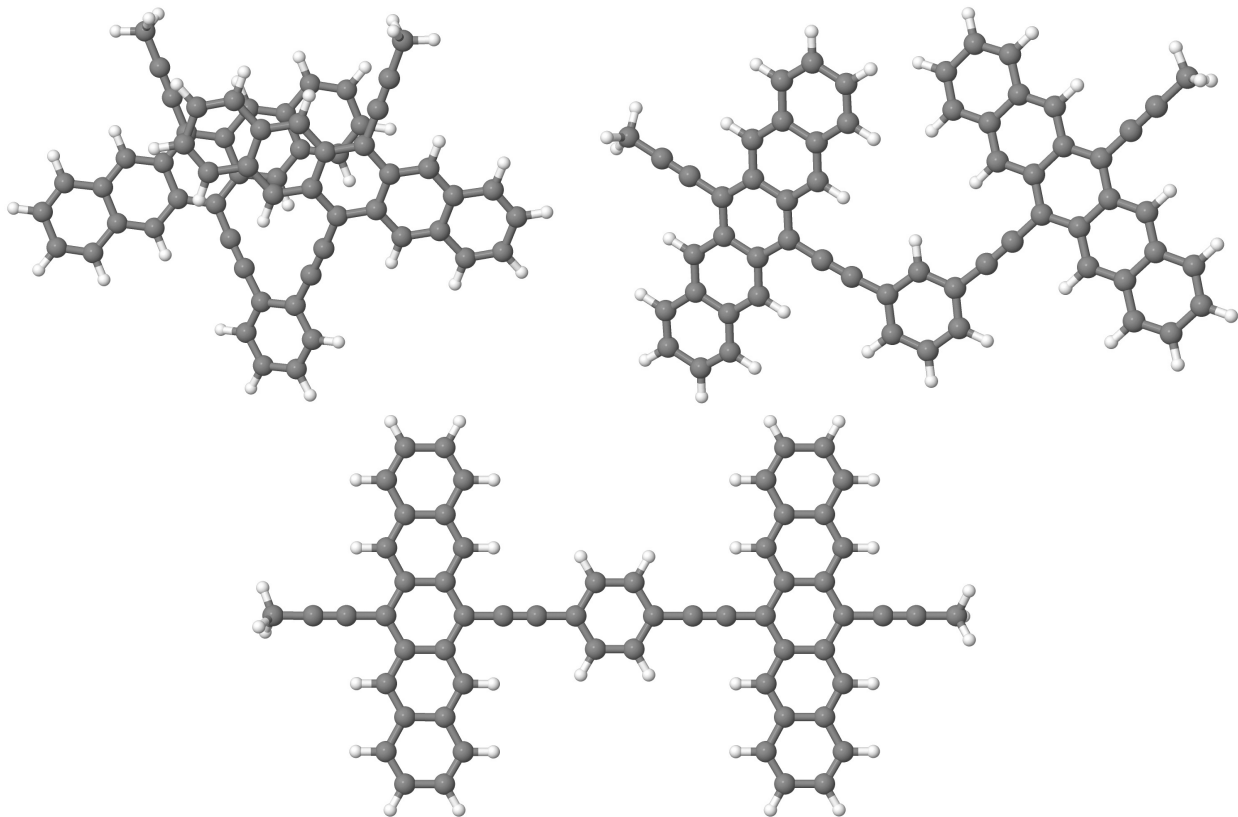

FIG. 1. Model systems investigated:o-TIPSPm (top, left), m-TIPSPm (top, right) and p-TIPSPm (bottom).

The vibronic model Hamiltonian was represented in a basis consisting of eight diabatic states relevant for the iSF process. These are the electronic ground state $|^1(S_0S_0)\rangle$, the locally excited (LE) states $|^1(S_0S_1)\rangle$ and $|^1(S_1S_0)\rangle$ where the excitation (S_1) is localized in one pentacene moiety, the ME (coupled triplet pair) state $|^1(T_1T_1)\rangle$, the CT states $|^1(CA)\rangle$ and $|^1(AC)\rangle$, where C and A stand for the radical cation and radical anion form of the pentacene moiety. Two doubly excited (DE) diabatic states $|^1(DE)_1\rangle$ and $|^1(DE)_2\rangle$ were also included on the basis of their energies and the potential role they may have in the mechanism of iSF in the systems investigated.[70] These states were built from the correspond-

ing adiabatic (mixed) electronic states employing the diabatization method of Nakamura and Truhlar.[105,106] For this, the adiabatic electronic states were calculated using the extended multiconfigurational quasidegenerate perturbation theory method (XMCQDPT)[107], a double-ζ (DZV) basis set[108] and employing an eight roots-equal weights state average complete active space self-consistent field (SA-CASSCF) calculation as reference. An active space of four electrons in four orbitals (HOMO and LUMO of each pentacene-like moiety) was used. To prevent the effect of intruder states in the energies of the states, an intruder state avoidance shift[109] of 0.02 was used (see Supporting Information for details).

The diabatic potential energy surfaces (see Eq. 2) were built using a combined approach that employs XMCQDPT energies and SA-CASSCF linear and quadratic coupling constants as described in ref. 70. As a consequence, the minimum of the ground state diabatic potential energy hypersurface does not coincide with the ground state equilibrium structure obtained at the DFT in all the systems investigated (see Supporting Information). Therefore, to prepare the initial wavepacket of our simulations we have shifted the equilibrium position of the normal modes to that of the ground state diabatic potential energy hypersurface and transformed the Q-dependent magnitudes when appropriate.

All the electronic structure calculations were carried out using TURBOMOLE[110] and GAMESS.[111,112] Quantum dynamics simulations were carried out using the Heidelberg MCTDH code.[113]

III. RESULTS AND DISCUSSION

In the following, we discuss the results obtained in the simulation of the early-events of the iSF process in the model systems o-, m- and p-TIPSPm using the theoretical methods described in the previous section.

A. Adiabatic and Diabatic Basis: Energies and Couplings

Table I shows the adiabatic vertical excitation energy, modulus of the dipole moment, oscillator strength and character of the lowest-lying singlet excited states of o-, m-, and p-TIPSPm calculated at the DFT optimized ground state equilibrium geometry. For all the systems investigated, state ordering is the same in the lower-energy part of the spectrum.

TABLE I. Adiabatic vertical excitation energy (ΔE, eV),[a] oscillator strength (f)[b], modulus of the dipole moment (μ, D)[b] and character (char.)[c] of the lowest-lying singlet excited states of o-,[d] m- and p-TIPSPm calculated at the ground state equilibrium structure.

State	o-TIPSPm				m-TIPSPm				p-TIPSPm			
	ΔE	f	μ	char.	ΔE	f	μ	char.	ΔE	f	μ	char.
S_1	1.51	<0.001	2.04	ME	1.79	<0.001	1.22	ME	1.72	<0.001	0.01	ME
S_2	1.75	1.003	2.48	LE	1.89	0.820	1.85	LE	1.84	1.488	0.01	LE
S_3	1.78	0.270	3.24	LE	1.95	0.450	1.85	LE	1.96	<0.001	0.01	LE
S_4	1.98	0.104	3.32	CT	2.16	<0.001	0.68	DE	2.17	<0.001	0.01	DE
S_5	2.00	<0.001	2.48	DE	2.32	0.002	0.67	DE	2.32	0.005	0.01	DE
S_6	2.20	0.001	1.54	DE	2.76	<0.001	23.52	CT	2.91	<0.001	0.03	CT
S_7	2.25	0.002	1.63	CT	2.77	0.002	23.50	CT	2.93	0.020	0.03	CT

[a] Calculated at the XMCQDPT/DZV level of theory (eight roots with equal weights and a four electrons in four orbitals active space were used in the CASSCF calculation).

[b] Calculated at the CASSCF/DZV level of theory (eight roots with equal weights and a four electrons in four orbitals active space were used).

[c] ME = multiexcitonic state, LE = optically bright and dark states that correlate with the plus and minus combinations of locally excited states at both pentacene monomers, CT = charge transfer states, DE = doubly excited states.

[d] Taken from ref. 70.

Specifically, the ME-like (S_1) state is the most stable, followed by two LE-like (S_2 and S_3) states. From the energetic point of view, these states are closely packed showing very similar vertical excitation energies in all systems, with the largest deviation found for the ME state of o-TIPSm, which differs from those of m- and p-TIPSPm by $\sim$0.28 eV and $\sim$0.21 eV, respectively. The vertical excitation energies of the LE-like states of o-TIPSm are also slightly more stable than those of m- and p-TIPSPm. All in all, o-TIPSPm exhibits energy gaps between the ME-like and the LE-like states slightly larger than those of m- and p-TIPSPm.

The remaining part of the spectrum contains both CT-like and DE-like states. Here, more significant changes are noted. First, there is a different state ordering in o-TIPSPm

TABLE II. Diabatic electronic Hamiltonian (H_{el}) containing the energies and coupling matrix elements (eV) of the low-lying diabatic electronic states used as basis for the simulation of the iSF process of o-TIPSPm calculated at the ground state equilibrium structure.[a,b]

H_{el}	$|^1(S_0S_0)\rangle$	$|^1(S_0S_1)\rangle$	$|^1(S_1S_0)\rangle$	$|^1(T_1T_1)\rangle$	$|^1(CA)\rangle$	$|^1(AC)\rangle$	$|^1(DE)_1\rangle$	$|^1(DE)_2\rangle$
$|^1(S_0S_0)\rangle$	0.0000	0.0150	−0.0149	−0.0180	−0.1078	0.1070	−0.4264	0.4166
$|^1(S_0S_1)\rangle$	0.0150	1.5767	0.0234	0.0070	−0.0308	−0.0432	0.0518	−0.0069
$|^1(S_1S_0)\rangle$	−0.0149	0.0234	1.5763	−0.0072	−0.0439	−0.0316	−0.0094	0.0513
$|^1(T_1T_1)\rangle$	−0.0180	0.0070	−0.0072	1.5949	−0.2727	0.2730	−0.0260	0.0240
$|^1(CA)\rangle$	−0.1078	−0.0308	−0.0439	−0.2727	1.7438	0.0257	0.0435	−0.0362
$|^1(AC)\rangle$	0.1070	−0.0432	−0.0316	0.2730	0.0257	1.7436	−0.0386	0.0418
$|^1(DE)_1\rangle$	−0.4264	0.0518	−0.0094	−0.0260	0.0435	−0.0386	1.8088	0.1765
$|^1(DE)_2\rangle$	0.4166	−0.0069	0.0513	0.0240	−0.0362	0.0418	0.1765	1.8210

[a] Taken from ref. 70.

[b] Calculated at the XMCQDPT/DZV level of theory (8 roots with equal weights and a 4 electrons in 4 orbitals active space were used in the CASSCF calculation).

with respect to those of m- and p-TIPSPm, with the former showing a CT-like state located ∼0.2 eV above the higher-lying LE-like state, followed by two DE-like states and another CT-like state. In contrast, both m- and p-TIPSPm exhibit DE-like states more stable than those CT-like. With respect to the vertical excitation energies, the DE-states show similar values (with differences smaller than ∼0.2 eV) in all the systems, indicating that they are relatively insensitive to the type of substitution ($ortho$, $meta$ and $para$) of the ground state equilibrium structure of the dimers. In contrast, the vertical excitation energies of the CT-like states show sizable changes among the different regiosomers, with those of o-TIPSPm being relatively low in energy and close to the rest of states whereas the energy gaps of these states in m- and p-TIPSPm are larger, as a consequence of the dependence of the energy of these states with the distance between positive and negative charges localized at each pentacene moiety.

Tables II–IV show the diabatic electronic Hamiltonians in the basis of diabatic states relevant for the iSF process (see Section II) of o-, m- and p-TIPSPm calculated at the corresponding ground state equilibrium structures. Similar to the results found for the

TABLE III. Diabatic electronic Hamiltonian (H_{el}) containing the energies and coupling matrix elements (eV) of the low-lying diabatic electronic states used as basis for the simulation of the iSF process of m-TIPSPm calculated at the ground state equilibrium structure.[a]

H_{el}	$\lvert^1(S_0S_0)\rangle$	$\lvert^1(T_1T_1)\rangle$	$\lvert^1(S_0S_1)\rangle$	$\lvert^1(S_1S_0)\rangle$	$\lvert^1(DE)_1\rangle$	$\lvert^1(DE)_2\rangle$	$\lvert^1(CA)\rangle$	$\lvert^1(AC)\rangle$
$\lvert^1(S_0S_0)\rangle$	0.0000	−0.0017	−0.0228	−0.0232	−0.4772	0.4656	0.0127	−0.0039
$\lvert^1(T_1T_1)\rangle$	−0.0017	1.5612	−0.0000	−0.0002	−0.0034	0.0030	0.0025	−0.0018
$\lvert^1(S_0S_1)\rangle$	−0.0228	−0.0000	1.6874	0.0324	−0.0433	0.0090	−0.0208	−0.0207
$\lvert^1(S_1S_0)\rangle$	−0.0232	−0.0002	0.0324	1.6874	−0.0114	0.0428	−0.0145	0.0193
$\lvert^1(DE)_1\rangle$	−0.4772	−0.0034	−0.0433	−0.0114	1.8867	0.1955	0.0060	−0.0031
$\lvert^1(DE)_2\rangle$	0.4656	0.0030	0.0090	0.0428	0.1955	1.9000	−0.0009	0.0052
$\lvert^1(CA)\rangle$	0.0127	0.0025	−0.0208	−0.0145	0.0060	−0.0009	2.5245	−0.0053
$\lvert^1(AC)\rangle$	−0.0039	−0.0018	−0.0207	0.0193	−0.0031	0.0052	−0.0053	2.5311

[a] Calculated at the XMCQDPT/DZV level of theory (8 roots with equal weights and a 4 electrons in 4 orbitals active space were used in the CASSCF calculation).

TABLE IV. Diabatic electronic Hamiltonian (H_{el}) containing the energies and coupling matrix elements (eV) of the low-lying diabatic electronic states used as basis for the simulation of the iSF process of p-TIPSPm calculated at the ground state equilibrium structure.[a]

H_{el}	$\lvert^1(S_0S_0)\rangle$	$\lvert^1(T_1T_1)\rangle$	$\lvert^1(S_0S_1)\rangle$	$\lvert^1(S_1S_0)\rangle$	$\lvert^1(DE)_1\rangle$	$\lvert^1(DE)_2\rangle$	$\lvert^1(CA)\rangle$	$\lvert^1(AC)\rangle$
$\lvert^1(S_0S_0)\rangle$	0.0000	0.0019	0.0217	0.0218	0.4743	−0.4628	−0.0439	0.0439
$\lvert^1(T_1T_1)\rangle$	0.0019	1.5346	−0.0010	−0.0011	−0.0380	0.0361	0.1812	−0.1813
$\lvert^1(S_0S_1)\rangle$	0.0217	−0.0010	1.6941	0.0404	−0.0108	0.0433	−0.1333	−0.1173
$\lvert^1(S_1S_0)\rangle$	0.0218	−0.0011	0.0404	1.6941	−0.0436	0.0088	0.1173	0.1339
$\lvert^1(DE)_1\rangle$	0.4743	−0.0380	−0.0108	−0.0436	1.8801	0.1923	0.0112	−0.0063
$\lvert^1(DE)_2\rangle$	−0.4628	0.0361	0.0433	0.0088	0.1923	1.8934	−0.0061	0.0113
$\lvert^1(CA)\rangle$	−0.0439	0.1812	−0.1333	0.1173	0.0112	−0.0061	2.6507	0.0098
$\lvert^1(AC)\rangle$	0.0439	−0.1813	−0.1173	0.1339	−0.0063	0.0113	0.0098	2.6507

[a] Calculated at the XMCQDPT/DZV level of theory (8 roots with equal weights and a 4 electrons in 4 orbitals active space were used in the CASSCF calculation).

adiabatic basis, both m- and p-TIPSPm show the same state ordering and very similar

state energies with the largest differences noted for the $|^1(CA)\rangle$ and $|^1(AC)\rangle$ states (~ 0.1 eV). In contrast, o-TIPSPm differs in the ordering of the states, with the $|^1(T_1T_1)\rangle$ state being slightly less stable than the $|^1(S_0S_1)\rangle$ and $|^1(S_1S_0)\rangle$ states and with the $|^1(CA)\rangle$ and $|^1(AC)\rangle$ states being significantly more stable than their m- and p-TIPSPm counterparts, which brings them close (< 0.2 eV energy gap) to $|^1(S_0S_1)\rangle$, $|^1(S_1S_0)\rangle$ and $|^1(T_1T_1)\rangle$ states.

With respect to the interstate electronic couplings, the built-in geometrical constraints imposed via o-, m- and p-substitution have an important impact on their magnitudes. In particular, the results show that the electronic couplings between the $|^1(T_1T_1)\rangle$ and the $|^1(S_0S_1)\rangle$ and $|^1(S_1S_0)\rangle$ states are negligible in m- and p-TIPSPm and small in o-TIPSPm. In contrast, the electronic couplings of these states with the CT states $|^1(CA)\rangle$ and $|^1(AC)\rangle$ are larger in all the systems. However, there is a remarkable difference in the values found for m-TIPSPm and those of o- and p-TIPSPm. Specifically, while m-TIPSPm shows negligible electronic coupling between $|^1(T_1T_1)\rangle$ and $|^1(CA)\rangle$, $|^1(AC)\rangle$ states, both o- and p-TIPSPm exhibit significant coupling, with that of o-TIPSPm being the largest. In addition, the couplings of the LE states $|^1(S_0S_1)\rangle$ and $|^1(S_1S_0)\rangle$ to the CT states in m-TIPSPm, despite being moderate, are again smaller than those found for o- and p-TIPSPm, with the latter showing values one order of magnitude larger than those of the rest of regioisomers. Regarding the doubly excited states $|^1(DE)_1\rangle$ and $|^1(DE)_2\rangle$, they exhibit similar couplings to $|^1(S_0S_1)\rangle$ and $|^1(S_1S_0)\rangle$ in all the regiosomers. In contrast, in m-TIPSPm these states exhibit smaller couplings to the CT states than those of o- and p-TIPSPm, although the differences with the $para$ isomer are minor. This trend is also noted for the couplings of $|^1(DE)_1\rangle$ and $|^1(DE)_2\rangle$ to the $|^1(T_1T_1)\rangle$ state, that are much smaller in m-TIPSPm than in o- and p-TIPSPm. This characteristic has a strong impact on the dynamics of the iSF in these systems (see subsection III C).

The latter also exhibit larger couplings of the DE states to the CT states than m-TIPSPm although the differences much smaller in m-TIPSPm than in o-TIPSPm although

trend and show, in general, smaller couplings in m-TIPSPm than in the other regioisomers. All in all, these results show that for the systems investigated, built-in geometrical constraints affecting the distance between chromophores and the existence of conjugation ($ortho$ and $para$) or cross-conjugation ($meta$) via the phenylene linker can be used to modulate the energies and couplings of the states involved in the iSF process.[34,49]
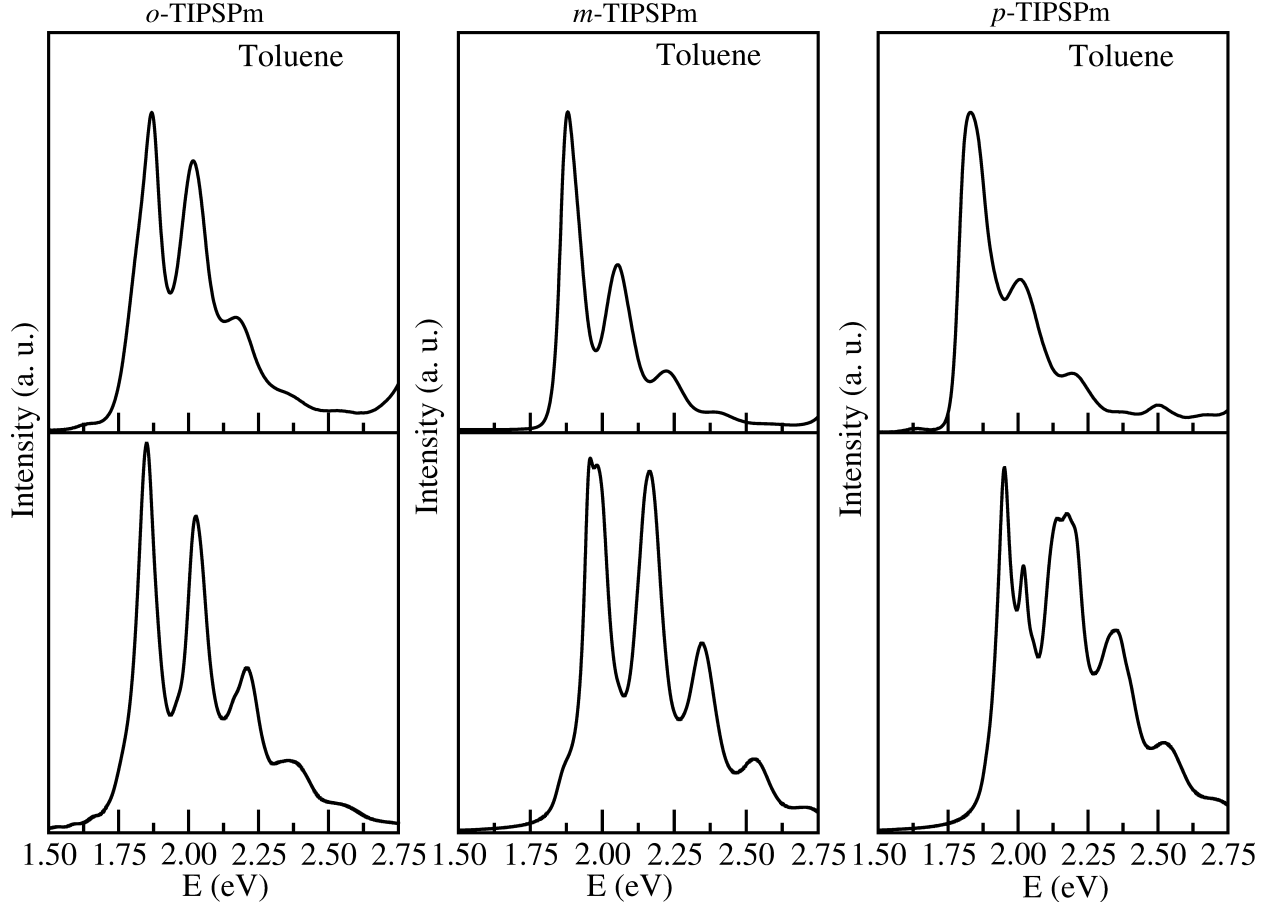
FIG. 2. Experimental (in toluene)[34] (top) and simulated (bottom) absorption spectra of the model systems o-, m- and p-TIPSPm in the range 1.50 eV to 2.75 eV. In the simulated spectra, the time-autocorrelation function obtained from the wavepacket propagation calculations has been damped with an exponential function ($e^{-\frac{t}{\tau}}$, with $\tau = 33$ fs) and Fourier transformed to generate the spectral envelope.

B.   Absorption Spectra

Fig. 2 depicts the absorption spectra of o-, m- and p-TIPSP measured in toluene[34] and those of o-,[70] m- and p-TIPSPm calculated using the Fourier transform of the time-autocorrelation function (see Eq. (7)). The results show good qualitative agreement between the experimental and calculates absorption spectra for the *ortho* and *meta* regioisomers in the energy range investigated. A typical vibrational progression is seen, which is characteristic of a pentacene-like structure, involving the vibrational modes ν_{19}, ν_{25} and ν_{27} in o-TIPSPm and ν_{16}, ν_{25} and ν_{29} in m-TIPSPm (see Supporting Information). Some differences exist, however,

in the relative intensity of the vibrational progression peaks, in particular in m-TIPSPm, and in the presence in the calculated spectra of m-TIPSPm of shoulder in the region $\sim$1.9 eV that is not observed in the experimental counterpart. Similar to o-TIPSPm, this feature originates from intensity borrowing from $|^1(S_1S_0)\rangle$ to $|^1(T_1T_1)\rangle$ states.[40] In contrast to these results, the differences found between the experimental and calculated absorption spectra of the *para* regioisomer are more significant. Although both spectra show the typical vibronic structure found in pentacene (involving ν_{16}, ν_{19} and ν_{24} vibrational modes), the calculated spectrum shows a Davydov splitting[114] of the main absorption peak that could be traced to the mix of CT states with the lowest-lying singlet excited states (see Supporting Material).[27] Furthermore, the weakly absorbing feature experimentally found in the near-infrared region is not present in the calculated spectra. These differences could stem from the limitations of the theoretical model, which does not account for the solvent effects of toluene, which are expected to have a more significant impact on the *para* regioisomer. In this respect, Müller *et al.*,[115] in their investigation of exciton fission and fusion in structurally related phenylene linked tetracene dimers, have pointed out that this type of systems exhibits small rotational barriers in solution (see also ref. 116), which enables the co-existence of different rotational conformations with very similar energies. Slight energy differences between these conformations would produce a broadening in the absorption spectra that we do not recover in our simulations allowing the observation of the Davidov splitting in p-TIPSPm.

C. Dynamics

Previous results obtained in the investigation of the dynamics of iSF in o-TIPSPm[70] demonstrated the instrumental role of electron-vibrational coupling in the process. There, it was shown that a model that only includes the electronic degrees of freedom (i.e. using a model Hamiltonian without coupling to vibrations) leads to Rabi-like oscillations between the two LE states $|^1(S_1S_0)\rangle$ and $|^1(S_0S_1)\rangle$ with negligible population of the ME state $|^1(T_1T_1)\rangle$. In the case of m- and p-TIPSPm, the electronic-only dynamics lead to the same result (see Supporting Information). Therefore, we have followed a similar approach for the investigation of the ultrafast dynamics of iSF in m- and p-TIPSPm and used the vibronic model Hamiltonian, Eq. (1), represented in the diabatic basis described above. Fig. 3 depicts the time evolution of the population of the different states considered in the iSF

process of o-, m- and p-TIPSPm in the first 600 fs after instantaneous photoexcitation of $|^1(S_1S_0)\rangle$. The results obtained show a clear dependence of the process on the structure of the molecules. Specifically, the largest population of the $|^1(T_1T_1)\rangle$ state is obtained for the *ortho* regioisomer, reaching a value of $\sim$70% at the end of the simulation time window explored, a value in line with results previously reported.[70] This is followed by the *para* regioisomer, for which the $|^1(T_1T_1)\rangle$ state population at 600 fs is close to 50%. In contrast to these regiosiomers, which show sizable populations of the $|^1(T_1T_1)\rangle$ state, the *meta* isomer shows a much smaller population for this state, reaching a value of $\sim$10% at the end of the simulation time. These results are in line with the trend experimentally found for these systems,[34] which predicted ultrafast population of the $|^1(T_1T_1)\rangle$ state in o-TIPSP and slower population of this state in p- and m-TIPSP.

Considering the short-time dynamics, in all the systems investigated, the initially populated $|^1(S_1S_0)\rangle$ state undergoes fast population transfer and exhibits already at $\sim$50 fs a population below $\sim$20%. Beyond this time, the decay is faster in o- and p-TIPSPm, with the former smoothly depopulating to values $\sim$5% at 600 fs and the latter showing some moderate revivals (damped Rabi-like oscillations involving the $|^1(S_0S_1)\rangle$ state reaching populations $\sim$30%) until $\sim$120 fs, when it starts a smooth decay to values below 10% at the end of the simulation time. The states involved in the population transfer in the short-time regime, on the other hand, do not significantly differ among the systems investigated. Specifically, in the three cases the initial dynamics prompts the population of $|^1(S_0S_1)\rangle$ $|^1(DE)_1\rangle$, $|^1(DE)_2\rangle$ and $|^1(S_0S_0)\rangle$ states. Only for o-TIPSPm, the $|^1(T_1T_1)\rangle$ state gets significantly populated in the short-time range (see Fig. 3(a)).

At longer simulation times, all systems show a steady increase of the population of $|^1(T_1T_1)\rangle$, more pronounced in o- and p-TIPSPm, while in m-TIPSPm the population of this state remains below those of the rest of states except for the CT ones, which are not significantly populated in any of the systems in the time-scale investigated. In this respect, o-TIPSPm exhibits the largest population of CT states. In addition, $|^1(T_1T_1)\rangle$ state exhibits small oscillations that are mirrored by the CT states at times beyond 150 fs (see Fig. 3(a)). This behavior is not observed in m-TIPSPm and to a very minor extent in p-TIPSPm. This is a consequence of the large energy gap of the CT states with respect to the $|^1(T_1T_1)\rangle$ state in these regiosomers, which is much larger than the characteristic vibrational energies of the modes included in the model.
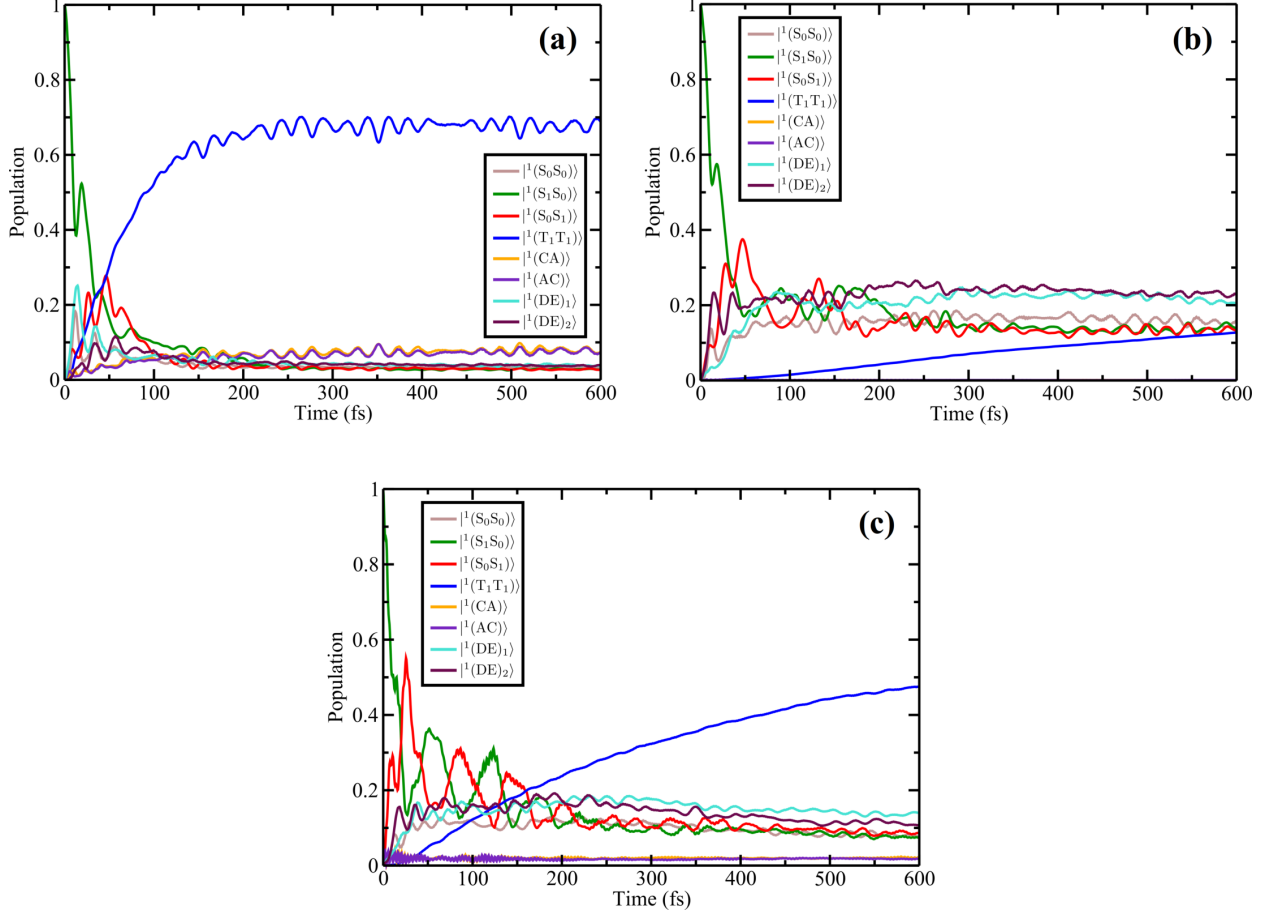
FIG. 3. Time evolution of the population of the diabatic states considered in the simulation of the iSF process of (a) o-, (b) m- and (c) p-TIPSPm. The calculations have been carried out assuming initial instantaneous photoexcitation of $|^1(S_1S_0)\rangle$.

To analyze the iSF mechanism and assess the contribution of the direct and mediated channels in m- and p-TIPSPm, we have followed a similar approach to that used in ref. 70 for o-TIPSPm. Specifically, we have simulated the dynamics of iSF using a series of vibronic model Hamiltonians that differ from the full models discussed before in the diabatic basis sets (i.e. in the number of diabatic states) used in the simulations (see Supporting Information for details). The results are depicted in Figs. 4 and 5. To analyze the contribution of the direct channel to the iSF mechanism, we have investigated the process using a vibronic model Hamiltonian represented in a basis that includes the $|^1(S_0S_0)\rangle$, $|^1(S_1S_0)\rangle$, $|^1(S_0S_1)\rangle$ and $|^1(T_1T_1)\rangle$ states. The results obtained, depicted in Figs. 4(a) and 5(a), show that the dynamics of the process is dominated by Rabi-like oscillations between the $|^1(S_1S_0)\rangle$ and $|^1(S_0S_1)\rangle$ states. In addition, the population of the $|^1(T_1T_1)\rangle$ state at the end of the
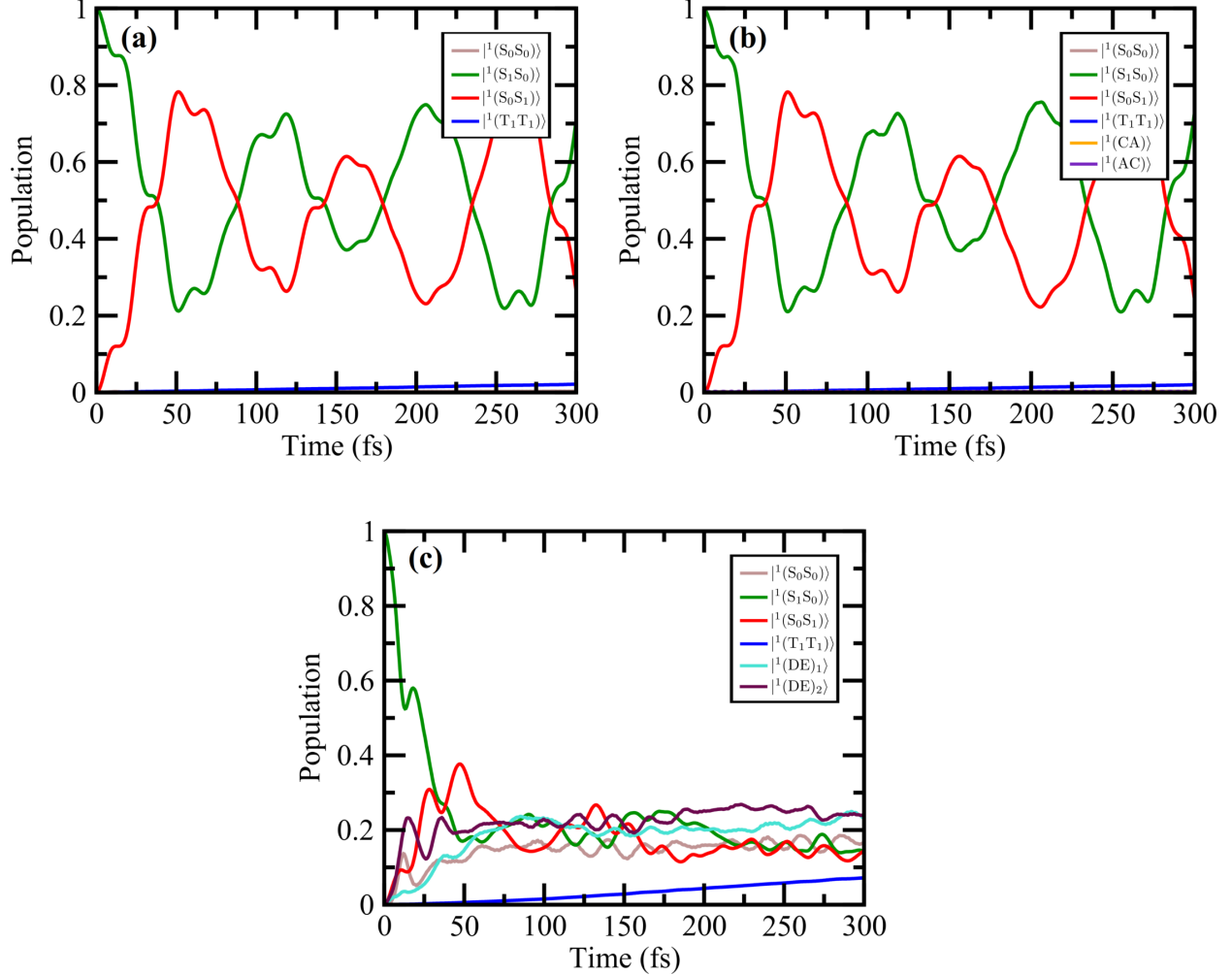
15

FIG. 4. Time evolution of the population of the diabatic states considered in the simulation of the iSF process of m-TIPSPm using vibronic model Hamiltonians represented in different diabatic basis sets ((a)–(c), see insets). The calculations have been carried out assuming initial instantaneous photoexcitation of $|^1(S_1S_0)\rangle$.

simulation time (300 fs) is negligible in m-TIPSPm and very small in p-TIPSPm leading to populations smaller than $\sim$5% at 300 fs. These results demonstrate that the contribution of the direct channel to the iSF mechanism is negligible for these systems, a fact in agreement with previous results obtained for o-TIPSPm.[70]

To investigate the mediated mechanism and to ascertain the role of the DE and CT states in the iSF process, we have analyzed the dynamics using basis sets that incorporate, in addition to the $|^1(S_0S_0)\rangle$, $|^1(S_1S_0)\rangle$, $|^1(S_0S_1)\rangle$ and $|^1(T_1T_1)\rangle$ states, $|^1(CA)\rangle$ and $|^1(AC)\rangle$ charge transfer states (see Figs. 4(b) and 5(b)) and the $|^1(DE)_1\rangle$ and $|^1(DE)_2\rangle$ doubly excited
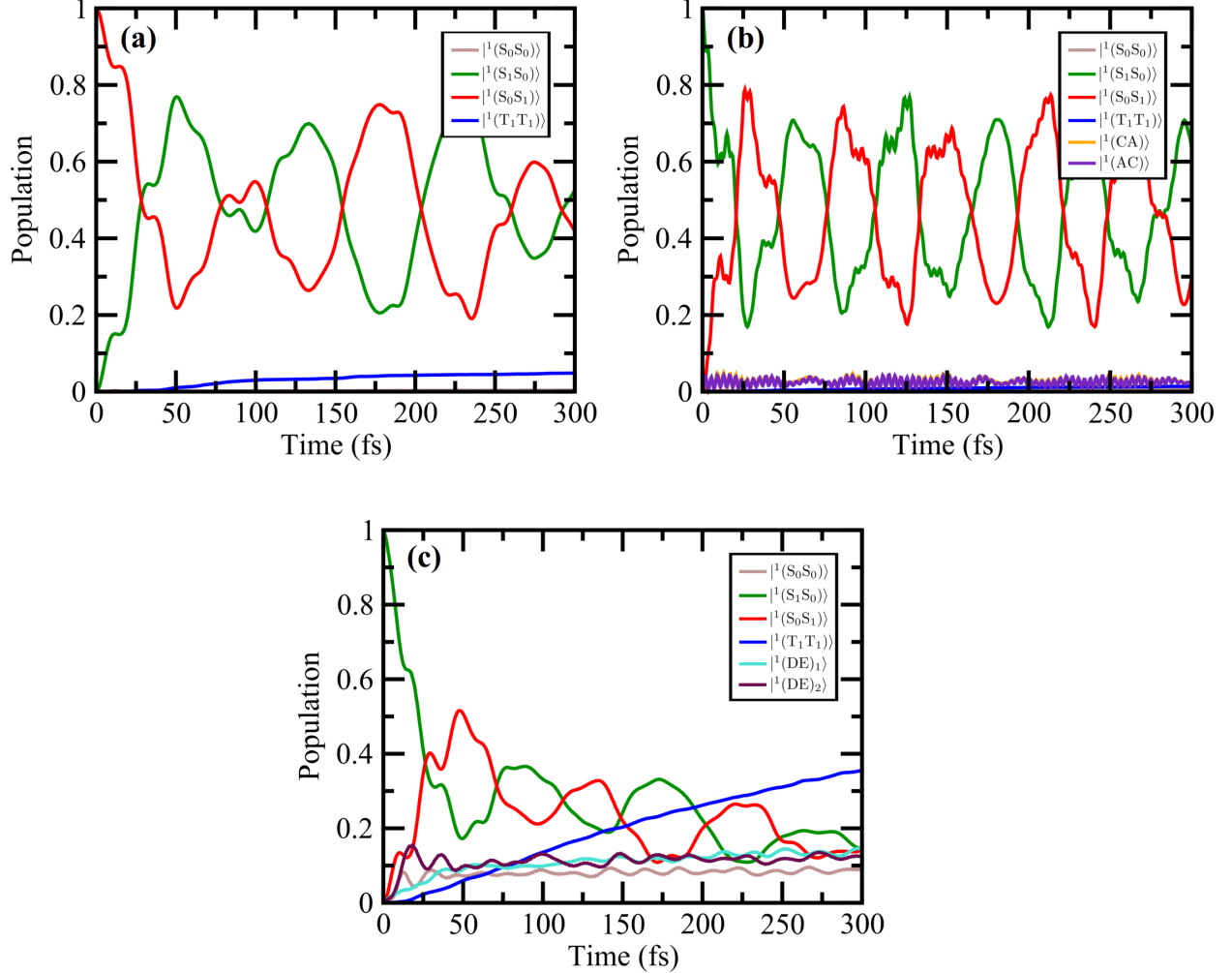
FIG. 5. Time evolution of the population of the diabatic states considered in the simulation of the iSF process of p-TIPSPm using vibronic model Hamiltonians represented in different diabatic basis sets ((a)–(c), see insets). The calculations have been carried out assuming initial instantaneous photoexcitation of $|^1(S_1 S_0)\rangle$.

states (see Figs. 4(c) and 5(c)). As can be observed, for both m- and p-TIPSPm the inclusion of CT states leads to very similar dynamics to those discussed before, with both regioisomers showing Rabi-like oscillations between the $|^1(S_1 S_0)\rangle$ and $|^1(S_0 S_1)\rangle$ states. In addition, very small population of the $|^1(T_1 T_1)\rangle$ state is again observed in the simulation time considered. Interestingly, this happens not only for the m-TIPSPm cross-conjugated system but also for p-TIPSPm that exhibits quite significant electronic couplings of the ME and LE states to the CT states. However, the contribution of these couplings to effective iSF is quenched by the large energy gap existing between the CT states and the ME and LE states in

both these regiosomers and also by the existence of destructive interference that leads to the cancellation of the pathways involving CT states.[64] These effects are not modified by changes in the couplings and energies of the states considered induced by the coupling to the molecular vibrations.

The addition of the two DE states to the reduced diabatic basis consisting of the $|^1(S_0S_0)\rangle$, $|^1(S_1S_0)\rangle$ $|^1(S_0S_1)\rangle$ and $|^1(T_1T_1)\rangle$ states has, on the other hand, a more significant effect. As can be observed in Figs. 4(c) and 5(c)), inclusion of the these states causes population of the $|^1(T_1T_1)\rangle$ state in both m- and p-TIPSPm, resulting in very similar dynamics to those obtained with the full model Hamiltonian in the range of times considered (300 fs).

This analysis shows that for these two regioisomers, where the CT states are too high in energy to contribute effectively to the process, the presence of lower-lying DE states provides an alternative mediated channel that allows the population of the $|^1(T_1T_1)\rangle$ state and therefore facilitates iSF. The slower dynamics exhibited by m-TIPSPm can be understood on the basis of the much smaller electronic couplings of $|^1(T_1T_1)\rangle$ to the DE states featured by this system. This is in line with the well-known interference effects affecting the magnitude of the bridge-mediated coupling contribution to the effective iSF coupling when the monomers in the dimer are bonded to an alternant hydrocarbon linker at two starred positions like in the case of $meta$.[117]

These results are in line with those obtained for o-TIPSPm, where the DE states were needed to trigger the population of the $|^1(T_1T_1)\rangle$ state due to the existence of destructive interference leading to cancellation of the pathways involving the CT states.[64] In the case of m- and p-TIPSPm, the simulations carried out with reduced vibronic model Hamiltonians point out that the relative contribution of the DE-mediated channel to the population of $|^1(T_1T_1)\rangle$ is significantly larger than those of the direct and the CT-mediated channels.

IV. CONCLUSIONS

We have investigated the dynamics of iSF in a series of pentacene-based dimers consisting of two pentacene-like chromophores covalently bonded to a phenylene linker in $ortho$, $meta$ and $para$ positions using a quantum dynamical approach that employs a model vibronic Hamiltonian whose parameters are obtained using multireference perturbation theory methods. The dimers were selected to get insight into the roles played by built-in geomet-

rical constraints and the electronic structure of the spacer in the iSF process. The results obtained, which qualitatively agree with the experimental data available, highlight the different contributions of the direct and mediated mechanism to the iSF process in the systems investigated. They show that the population of the ME state, corresponding to the first step of the iSF process, occurs mainly through a mediated (superexchange-like) mechanism. However, our results also point out that the presence of lower-lying DE states provide an alternative mediated channel to that involving CT states that allows the population of the ME state and therefore facilitates the iSF process. In addition, our results indicate that substitution in *ortho*, *meta* and *para* can be used to control the relative energy of the CT states and to modulate the magnitude of the electronic couplings that are smaller for the *meta* regioisomer, where the pentacene-like monomers are cross-conjugated through the phenylene linker. All in all, these results provide information to rationalize the effects that built-in geometrical constraints have in the iSF process and suggest new ways of enhancing iSF through the control of the relative energies of DE and CT states employing chemical substitution or solvent effects.

V. SUPPLEMENTARY MATERIAL

See supplementary material for further details on the electronic structure and quantum dynamical methods, characterization of the different electronic states included in the simulations and for the list of parameters used to build the vibronic Hamiltonians.

REFERENCES

[1] M. B. Smith and J. Michl, Chem. Rev. **110**, 6891 (2010).

[2] D. Casanova, Chem. Rev. **118**, 7164 (2018).

[3] A. Japahuge and T. Zeng, ChemPlusChem **83**, 146 (2018).

[4] S. Singh, W. J. Jones, W. Siebrand, B. P. Stoicheff, and W. G. Schneider, J. Chem. Phys. **42**, 330 (1965).

[5] C. Swenberg and W. Stacy, Chem. Phys. Lett. **2**, 327 (1968).

[6] A. J. Nozik, R. J. Ellingson, O. I. Micic, J. L. Blackburn, P. Yu, J. E. Murphy, M. C. Beard, and G. Rumbles, in *Proc. 27th DOE Solar Photochem. Res. Conf.* (U.S. Dep. Energy, 2004) pp. 63–66.

[7] M. C. Hanna and A. J. Nozik, J. Appl. Phys. **100**, 074510 (2006).

[8] R. D. Schaller and V. I. Klimov, Phys. Rev. Lett. **92**, 186601 (2004).

[9] D. N. Congreve, J. Lee, N. J. Thompson, E. Hontz, S. R. Yost, P. D. Reusswig, M. E. Bahlke, S. Reineke, T. Van Voorhis, and M. A. Baldo, Science **340**, 334 (2013).

[10] J. Xia, S. N. Sanders, W. Cheng, J. Z. Low, J. Liu, L. M. Campos, and T. Sun, Adv. Mater. **29**, 1601652 (2017).

[11] W. Shockley and H. J. Queisser, J. Appl. Phys. **32**, 510 (1961).

[12] B. J. Walker, A. J. Musser, D. Beljonne, and R. H. Friend, Nat. Chem. **5**, 1019 (2013).

[13] M. B. Smith and J. Michl, Ann. Rev. Phys. Chem. **64**, 361 (2013).

[14] J. J. Burdett and C. J. Bardeen, Acc. Chem. Res. **46**, 1312 (2013).

[15] A. A. Bakulin, S. E. Morgan, T. B. Kehoe, M. W. B. Wilson, A. W. Chin, D. Zigmantas, D. Egorova, and A. Rao, Nat. Chem. **8**, 16 (2015).

[16] C. E. Swenberg and N. E. Geacintov, "Exciton interactions in organic solids," in *Organic Molecular Photophysics*, Wiley monographs in chemical physics, Vol. 1, edited by J. B. Birks (Wiley, New York, 1973) Chap. 10, pp. 489–564.

[17] H. Benk and H. Sixl, Mol. Phys. **42**, 779 (1981).

[18] J. J. Burdett, G. B. Piland, and C. J. Bardeen, Chem. Phys. Lett. **585**, 1 (2013).

[19] G. B. Piland, J. J. Burdett, R. J. Dillon, and C. J. Bardeen, J. Phys. Chem. Lett. **5**, 2312 (2014).

[20] G. D. Scholes, J. Phys. Chem. A **119**, 12699 (2015).

[21]L. R. Weiss, S. L. Bayliss, F. Kraffert, K. J. Thorley, J. E. Anthony, R. Bittl, R. H. Friend, A. Rao, N. C. Greenham, and J. Behrends, Nat. Phys. **13**, 176 (2016).

[22]M. J. Y. Tayebjee, S. N. Sanders, E. Kumarasamy, L. M. Campos, M. Y. Sfeir, and D. R. McCamey, Nat. Phys. **13**, 182 (2016).

[23]B. S. Basel, J. Zirzlmeier, C. Hetzer, B. T. Phelan, M. D. Krzyaniak, S. R. Reddy, P. B. Coto, N. E. Horwitz, R. M. Young, F. J. White, F. Hampel, T. Clark, M. Thoss, R. R. Tykwinski, M. R. Wasielewski, and D. M. Guldi, Nat. Commun. **8**, 15171 (2017).

[24]B. S. Basel, J. Zirzlmeier, C. Hetzer, S. R. Reddy, B. T. Phelan, M. D. Krzyaniak, M. K. Volland, P. B. Coto, R. M. Young, T. Clark, M. Thoss, R. R. Tykwinski, M. R. Wasielewski, and D. M. Guldi, Chem **4**, 1092 (2018).

[25]R. Casillas, M. Adam, P. B. Coto, A. R. Waterloo, J. Zirzlmeier, S. R. Reddy, F. Hampel, R. McDonald, R. R. Tykwinski, M. Thoss, and D. M. Guldi, Adv. Energy Mater. **9**, 1802221 (2019).

[26]P. M. Zimmerman, Z. Zhang, and C. B. Musgrave, Nat. Chem. **2**, 648 (2010).

[27]D. Beljonne, H. Yamagata, J. L. Brédas, F. C. Spano, and Y. Olivier, Phys. Rev. Lett. **110**, 226402 (2013).

[28]W.-L. Chan, T. C. Berkelbach, M. R. Provorse, N. R. Monahan, J. R. Tritsch, M. S. Hybertsen, D. R. Reichman, J. Gao, and X.-Y. Zhu, Acc. Chem. Res. **46**, 1321 (2013).

[29]X. Feng, A. V. Luzanov, and A. I. Krylov, J. Phys. Chem. Lett. **4**, 3845 (2013).

[30]P. M. Zimmerman, C. B. Musgrave, and M. Head-Gordon, Acc. Chem. Res. **46**, 1339 (2013).

[31]D. Casanova, J. Chem. Theory Comput. **10**, 324 (2014).

[32]T. Zeng, R. Hoffmann, and N. Ananth, J. Am. Chem. Soc. **136**, 5755 (2014).

[33]P. B. Coto, S. Sharifzadeh, J. B. Neaton, and M. Thoss, J. Chem. Theory Comput. **11**, 147 (2015).

[34]J. Zirzlmeier, D. Lehnherr, P. B. Coto, E. T. Chernick, R. Casillas, B. S. Basel, M. Thoss, R. R. Tykwinski, and D. M. Guldi, Proc. Natl. Acad. Sci. U.S.A. **112**, 5325 (2015).

[35]F. Mirjani, N. Renaud, N. Gorczak, and F. C. Grozema, J. Phys. Chem. C **118**, 14192 (2014).

[36]P. Petelenz, M. Snamina, and G. Mazur, J. Phys. Chem. C **119**, 14338 (2015).

[37]E. G. Fuemmeler, S. N. Sanders, A. B. Pun, E. Kumarasamy, T. Zeng, K. Miyata, M. L. Steigerwald, X.-Y. Zhu, M. Y. Sfeir, L. M. Campos, and N. Ananth, ACS Cent. Sci. **2**,

316 (2016).

[38] S. Izadnia, D. W. Schnleber, A. Eisfeld, A. Ruf, A. C. LaForge, and F. Stienkemeier, J. Phys. Chem. Lett. **8**, 2068 (2017), pMID: 28421765.

[39] J. Ren, Q. Peng, X. Zhang, Y. Yi, and Z. Shuai, J. Phys. Chem. Lett. **8**, 2175 (2017).

[40] R. Tempelaar and D. R. Reichman, J. Chem. Phys. **146**, 174703 (2017).

[41] K. Miyata, F. S. Conrad-Burton, F. L. Geyer, and X.-Y. Zhu, Chem. Rev. **119**, 4261 (2019).

[42] R. W. Havenith, H. D. de Gier, and R. Broer, Mol. Phys. **110**, 2445 (2012).

[43] T. C. Berkelbach, M. S. Hybertsen, and D. R. Reichman, J. Chem. Phys. **138**, 114103 (2013).

[44] P. J. Vallett, J. L. Snyder, and N. H. Damrauer, J. Phys. Chem. A **117**, 10824 (2013).

[45] S. M. Parker, T. Seideman, M. A. Ratner, and T. Shiozaki, J. Phys. Chem. C **118**, 12700 (2014).

[46] S. R. Yost, J. Lee, M. W. B. Wilson, T. Wu, D. P. McMahon, R. R. Parkhurst, N. J. Thompson, D. N. Congreve, A. Rao, K. Johnson, M. Y. Sfeir, M. G. Bawendi, T. M. Swager, R. H. Friend, M. A. Baldo, and T. Van Voorhis, Nat. Chem. **6**, 492 (2014).

[47] N. Renaud and F. C. Grozema, J. Phys. Chem. Lett. **6**, 360 (2015).

[48] C.-H. Yang and C.-P. Hsu, J. Phys. Chem. Lett. **6**, 1925 (2015).

[49] J. Zirzlmeier, R. Casillas, S. R. Reddy, P. B. Coto, D. Lehnherr, E. T. Chernick, I. Papadopoulos, M. Thoss, R. R. Tykwinski, and D. M. Guldi, Nanoscale **8**, 10113 (2016).

[50] S. Ito, T. Nagami, and M. Nakano, RSC Adv. **7**, 34830 (2017).

[51] S. R. Reddy, P. B. Coto, and M. Thoss, Chem. Phys. **515**, 628 (2018).

[52] E. C. Greyson, J. Vura-Weis, J. Michl, and M. A. Ratner, J. Phys. Chem. B **114**, 14168 (2010).

[53] W. Mou, S. Hattori, P. Rajak, F. Shimojo, and A. Nakano, Appl. Phys. Lett. **102**, 173301 (2013).

[54] A. V. Akimov and O. V. Prezhdo, J. Am. Chem. Soc. **136**, 1599 (2014).

[55] L. Wang, Y. Olivier, O. V. Prezhdo, and D. Beljonne, J. Phys. Chem. Lett. **5**, 3345 (2014).

[56] G. Tao, J. Phys. Chem. C **118**, 17299 (2014).

[57] G. Tao, J. Phys. Chem. C **118**, 27258 (2014).

[58] G. Tao, J. Chem. Theory Comput. **11**, 28 (2015).

[59] A. D. Chien, A. R. Molina, N. Abeyasinghe, O. P. Varnavski, T. Goodson, and P. M. Zimmerman, J. Phys. Chem. C **119**, 28258 (2015).

[60] H. Tamura, M. Huix-Rotllant, I. Burghardt, Y. Olivier, and D. Beljonne, Phys. Rev. Lett. **115**, 107401 (2015).

[61] Y. Fujihashi and A. Ishizaki, J. Phys. Chem. Lett. **7**, 363 (2016).

[62] M. Nakano, S. Ito, T. Nagami, Y. Kitagawa, and T. Kubo, J. Phys. Chem. C **120**, 22803 (2016).

[63] J. Zheng, Y. Xie, S. Jiang, and Z. Lan, J. Phys. Chem. C **120**, 1375 (2016).

[64] M. A. Castellanos and P. Huo, J. Phys. Chem. Lett. **8**, 2480 (2017).

[65] Y. Fujihashi, L. Chen, A. Ishizaki, J. Wang, and Y. Zhao, J. Chem. Phys. **146**, 044101 (2017).

[66] Z. Huang, Y. Fujihashi, and Y. Zhao, J. Phys. Chem. Lett. **8**, 3306 (2017).

[67] A. F. Morrison and J. M. Herbert, J. Phys. Chem. Lett. **8**, 1442 (2017).

[68] S. Prodhan and S. Ramasesha, Phys. Rev. B **96**, 075142 (2017).

[69] H. Zang, Y. Zhao, and W. Liang, J. Phys. Chem. Lett. **8**, 5105 (2017).

[70] S. R. Reddy, P. B. Coto, and M. Thoss, J. Phys. Chem. Lett. **9**, 5979 (2018).

[71] R. Tempelaar and D. R. Reichman, J. Chem. Phys. **148**, 244701 (2018).

[72] M. Wei, F. Jin, T. Chen, H. Ma, C. Liu, and Y. Ma, J. Phys. Chem. C **123**, 3541 (2019).

[73] M. Wibowo, M. Persico, and G. Granucci, Phys. Chem. Chem. Phys. **21**, 692 (2019).

[74] X. Xie, A. Santana-Bonilla, W. Fang, C. Liu, A. Troisi, and H. Ma, J. Chem. Theory Comput. **15**, 3721 (2019).

[75] A. Akdag, Z. Havlas, and J. Michl, J. Am. Chem. Soc. **134**, 14624 (2012).

[76] T. Minami, S. Ito, and M. Nakano, J. Phys. Chem. Lett. **3**, 2719 (2012).

[77] T. Minami, S. Ito, and M. Nakano, J. Phys. Chem. Lett. **4**, 2133 (2013).

[78] N. Renaud, P. A. Sherratt, and M. A. Ratner, J. Phys. Chem. Lett. **4**, 1065 (2013).

[79] X. Feng, A. B. Kolomeisky, and A. I. Krylov, J. Phys. Chem. C **118**, 19608 (2014).

[80] T. Zeng, N. Ananth, and R. Hoffmann, J. Am. Chem. Soc. **136**, 12638 (2014).

[81] S. Ito and M. Nakano, J. Phys. Chem. C **119**, 148 (2015).

[82] T. Zeng and P. Goel, J. Phys. Chem. Lett. **7**, 1351 (2016).

[83] T. Zeng, J. Phys. Chem. Lett. **7**, 4405 (2016).

[84] T. C. Berkelbach, "Electronic structure and dynamics of singlet fission in organic molecules and crystals," in *Advances in Chemical Physics*, Vol. 162 (John Wiley & Sons,

Ltd, 2017) Chap. 1, pp. 1–38.

[85]N. Monahan and X.-Y. Zhu, Annu. Rev. Phys. Chem. **66**, 601 (2015).

[86]A. J. Musser, M. Maiuri, D. Brida, G. Cerullo, R. H. Friend, and J. Clark, J. Am. Chem. Soc. **137**, 5130 (2015).

[87]L. Yang, M. Tabachnyk, S. L. Bayliss, M. L. Böhm, K. Broch, N. C. Greenham, R. H. Friend, and B. Ehrler, Nano Lett. **15**, 354 (2015).

[88]E. Kumarasamy, S. N. Sanders, M. J. Y. Tayebjee, A. Asadpoordarvish, T. J. H. Hele, E. G. Fuemmeler, A. B. Pun, L. M. Yablon, J. Z. Low, D. W. Paley, J. C. Dean, B. Choi, G. D. Scholes, M. L. Steigerwald, N. Ananth, D. R. McCamey, M. Y. Sfeir, and L. M. Campos, J. Am. Chem. Soc. **139**, 12488 (2017).

[89]H. Yamagata, J. Norton, E. Hontz, Y. Olivier, D. Beljonne, J. L. Brédas, R. J. Silbey, and F. C. Spano, J. Chem. Phys. **134**, 204703 (2011).

[90]H. Köppel, W. Domcke, and L. S. Cederbaum, Adv. Chem. Phys. **57**, 59 (1984).

[91]H.-D. Meyer, U. Manthe, and L. Cederbaum, Chem. Phys. Lett. **165**, 73 (1990).

[92]M. Beck, A. Jäckle, G. Worth, and H.-D. Meyer, Phys. Rep. **324**, 1 (2000).

[93]H. Wang and M. Thoss, J. Chem. Phys. **119**, 1289 (2003).

[94]U. Manthe, J. Chem. Phys. **128**, 164116 (2008).

[95]H.-D. Meyer, F. Gatti, and G. A. Worth, eds., *Multidimensional Quantum Dynamics* (Wiley-VCH Verlag GmbH & Co., Weinheim, 2009).

[96]O. Vendrell and H.-D. Meyer, J. Chem. Phys. **134**, 044135 (2011).

[97]H. Wang, J. Phys. Chem. A **119**, 7951 (2015).

[98]H. Wang and M. Thoss, J. Chem. Phys. **145**, 164105 (2016).

[99]S. H. Vosko, L. Wilk, and M. Nusair, Can. J. Phys. **58**, 1200 (1980).

[100]A. D. Becke, Phys. Rev. A **38**, 3098 (1988).

[101]C. Lee, W. Yang, and R. G. Parr, Phys. Rev. B **37**, 785 (1988).

[102]A. D. Becke, J. Chem. Phys. **98**, 5648 (1993).

[103]F. Weigend and R. Ahlrichs, Phys. Chem. Chem. Phys. **7**, 3297 (2005).

[104]S. Grimme, J. Antony, S. Ehrlich, and H. Krieg, J. Chem. Phys. **132**, 154104 (2010).

[105]H. Nakamura and D. G. Truhlar, J. Chem. Phys. **115**, 10353 (2001).

[106]H. Nakamura and D. G. Truhlar, J. Chem. Phys. **117**, 5576 (2002).

[107]A. A. Granovsky, J. Chem. Phys. **134**, 214113 (2011).

[108] T. H. Dunning and P. J. Hay, "Gaussian basis sets for molecular calculations," in *Methods of Electronic Structure Theory*, Modern Theoretical Chemistry, Vol. 3, edited by H. F. Schaefer III (Springer US, New York, 2013) Chap. 1, pp. 1–27.

[109] H. A. Witek, Y.-K. Choe, J. P. Finley, and K. Hirao, J. Comput. Chem. **23**, 957 (2002).

[110] "TURBOMOLE V7.0 2015, a development of University of Karlsruhe and Forschungszentrum Karlsruhe GmbH, 1989-2007, TURBOMOLE GmbH, since 2007; available from *http://www.turbomole.com*.".

[111] M. W. Schmidt, K. K. Baldridge, J. A. Boatz, S. T. Elbert, M. S. Gordon, J. H. Jensen, S. Koseki, N. Matsunaga, K. A. Nguyen, S. Su, T. L. Windus, M. Dupuis, and J. A. Montgomery, J. Comput. Chem. **14**, 1347 (1993).

[112] M. S. Gordon and M. W. Schmidt, "Advances in electronic structure theory: Gamess a decade later," in *Theory and Applications of Computational Chemistry: the first forty years*, edited by C. E. Dykstra, G. Frenking, K. S. Kim, and G. E. Scuseria (Elsevier, 2005) Chap. 41, pp. 1167–1189.

[113] "The Heidelberg MCTDH package, version 8.5 (2011)." Available from *http://mctdh.uni-hd.de*.

[114] A. Davydov, *Theory of Molecular Excitons* (Springer US, 2013).

[115] A. M. Müller, Y. S. Avlasevich, W. W. Schoeller, K. Müllen, and C. J. Bardeen, J. Am. Chem. Soc. **129**, 14240 (2007).

[116] N. V. Korovina, J. Joy, X. Feng, C. Feltenberger, A. I. Krylov, S. E. Bradforth, and M. E. Thompson, J. Am. Chem. Soc. **140**, 10179 (2018).

[117] S. Ito, T. Nagami, and M. Nakano, J. Phys. Chem. A **120**, 6236 (2016).